Journal Name

ARTICLE

Pyrene-Functionalized Polymeric Carbon Nitride with Promoted Aqueous-Organic Biphasic Photocatalytic CO_2 Reduction

Xuezhong Gong,[a] Sijia Yu,[a] Meili Guan,[b] Xianglin Zhu[a] and Can Xue,*[a]

Received 00th January 20xx,
Accepted 00th January 20xx

DOI: 10.1039/x0xx00000x

www.rsc.org/

We have demonstrated a simple copolymerization process to covalently graft pyrene-functional groups on the polymeric carbon nitride (PCN) surface. The resulted pyrene functionalized carbon nitride (Py-PCN) exhibits unique biphasic photocatalytic activities, which enables efficient CO_2 photoreduction in the aqueous solution with simultaneous alkene (C=C) oxidation in the organic phase. The great biphasic activities are attributed to the increased lipophilicity from surface pyrene-functional groups that allows the hydrophobic alkene molecules to readily approach the PCN surface, and be reacted with the hydroxyl radicals created from –OH oxidaion by photogeneratd holes. By this way, the alkene compounds indirectly consume the photo-holes from excited Py-PCN, promoting the overall photocatalytic processes. Our studies provide a new strategy of solar fuels production with simultaneous organic synthesis by the oxidization power of photo-holes on amphiphilic metal-free semiconductors.

1. Introduction

Considering the increasing CO_2 concentration in atmosphere and over consumption of fossil fuels, photocatalytic CO_2 conversion to value-added fuels is believed as an effective way to alleviate the energy crisis and environmental issues.[1] Among all the semiconductors that are capable of reducing CO_2, polymeric carbon nitride (PCN) attracted most of the research interest due to its perfect band structure.[2] Specifically, its high conduction band with respect to the CO_2 reduction potentials provides thermodynamic driving force. And the versatile strategies for PCN structure modification, such as copolymerization,[3] heterojunction,[4-6] and elemental doping,[7] can be smoothly applied to functionalize PCN for boosting its photocatalytic activity of CO_2 reduction. Moreover, PCN features amphiphilic property owing to the terminal amine groups [8], enabling excellent affinity to the absorbates in aqueous solution for surface reaction.

To date, most photocatalytic CO_2 reduction tests were carried out in aqueous suspensions, in which H_2O is expected to serve as the electron donor.[9,10] In principle, the potential of the photohole (E_{vb} = +1.4 V, vs. NHE) of PCN is capable for water oxidation into O_2 (E_{H_2O/O_2} = +1.23 V, vs NHE). However, the large overpotential for O_2 evolution makes the real O_2 generation on PCN surface very difficult. As such, some sacrificial reagents, such as triethanolamine (TEOA), were commonly used for the photocatalytic CO_2 reduction.[11] Further, in terms of photocatalytic pollutant degradation, PCN was capable of oxidizing phenol,[12] bisphenol A[13] and some organic dyes by hydroxyl radicals and/or superoxide radicals.[14] Considering π–conjugated units in the PCN backbones,[15] the π–conjugated molecules (*e.g.*, alkene, alkyne and aromatics) could be preferably adsorbed via interfacial π–π conjugation. Nevertheless, this requires the PCN being capable of dispersing in organic solvents in order to attain optimal adsorption for those π–conjugated molecules.

Co-polymerization of PCN precursors with co-monomers (*e.g.*, 2-aminobenzonitrile, aniline, benzonitrile, *etc.*) was commonly used to obtain functionalized PCN.[16-18] However, the co-polymerization usually inserted the functional group into the PCN matrix, which significantly altered the PCN band structures beside the surface properties. An alternative strategy is post-calcination of PCN mixed with functional molecules, which is not effective with non-uniform surface functionalization. The required high temperature calcination restricted the available range of monomers in particular with large conjugated units that may decompose or carbonize.

According to our previous studies, the PCN can be formed through a solvothermal process, which allows for covalent attachment of triazine-based oligomers on the surface.[19] Such oligomers can be further condensed upon mild annealing.[20] These observations suggest that the conjugated functional groups on triazine-based molecules can be covalently linked onto PCN surface via post-polymerization to modulate the surface properties.

Specifically, in this work, we introduce surface pyrene-functionalization on PCN through a solvothermal process by using 1-(4,6-dichloro-1,3,5-triazin-2-yl)pyrene (PyCC) as the monomer and pre-synthesized PCN microspheres as the matrix. The heptazine units in PCN are naturally hydrophilic, which allows it to readily disperse in water. While the pyrene-moiety

[a] School of Materials Science and Engineering, Nanyang Technological University, 50 Nanyang Avenue, 639798 Singapore.
[b] Institute for Energy Research, Jiangsu University, 301 Xuefu Road, Zhejiang, 212013, P. R. China.

Electronic Supplementary Information (ESI) available: See DOI: 10.1039/x0xx00000x

supplies hydrophobic sites that allows affinity in nonpolar solvent for adsorption and reaction of organic compounds.

As such, the pyrene-functionalized polymeric carbon nitride (Py-PCN) can act as an aqueous-organic biphasic photocatalyst, which enables photoreduction of bicarbonate in aqueous phase and simultaneous oxidation of organic compounds in a non-polar solvent. Here, for proof-of-concept, we demonstrate that the photogenerated holes of PCN can lead to oxidation of C=C bond of alkene compounds, while the pyrene group on Py-PCN can greatly enhance the affinity of alkene compounds in organic phase and allows for more effective oxidation reaction. This work provide valuable guidance for design and preparation of multifunctional PCN photocatalysts for not only CO_2 reduction but also simultaneous organic synthesis in nonpolar organic solvents.

2. Experimental

2.1 Chemicals:

All the chemical reagents were used as received without further purification. Cyanuric chloride (99%), cyanamide (99%), 1-(4,6-Dichloro-1,3,5-triazin-2-yl)pyrene (≥85%), sodium bicarbonate (99.5%), cyclohexene (>99.7), 2-Methyl-2-butene (>99.0%), acetonitrile (anhydrous, 99.8%), toluene (HPLC Plus,≥99.9%) were all purchased from Sigma-Aldrich.

2.2. Synthesis of polymeric carbon nitride:

The raw PCN was synthesized through a solvothermal approach. Typically, 360 mg cyanuric chloride (**CC**) and 168 mg cyanimide (**CA**) dissolved in 15 mL acetonitrile through sonication, which was transferred into a 40-ml Teflon-lined auto-clave. Afterwards, the autoclave was sealed, put into an oven, and maintained at 200 ˚C for 24 h. The obtained products were washed with acetonitrile, DI water and absolute ethanol in sequence, and finally dried at 80 ˚C. This raw PCN sample is denoted as **CN0**.

2.3. Synthesis of pyrene-functionalized polymeric carbon nitride (Py-PCN):

The synthesized **CN0** (100 mg) was dispersed in acetonitrile to form a homogeneous suspension. Different amount of 1-(4,6-Dichloro-1,3,5-triazin-2-yl)pyrene (**PyCC**) were added into the suspension together with **CC** and **CA**. The molar ratio of **PyCC** : **CC** : **CA** is 1:1:5. The mixture was transferred to a Teflon-line autoclave that was placed in an oven maintaining at 200 ˚C for 24 h. The obtained products were washed with acetonitrile, DI water and absolute ethanol in sequence and finally and dried at 80 ˚C. The final Py-PCN samples was labelled as 2.5% Py-PCN, 5% Py-PCN, 10% Py-PCN and 20% Py-PCN based on the mass ratio of **PyCC** to **CN0**. As a control sample, the CN0 was treated with the same solvothermal process in acetonitrile with only CC and CA (no PyCC), which is considered as the bare PCN and denoted as **0-PCN**.

2.4. Characterization:

SEM images were obtained by FESEM 7600F scanning electron microscope set 5 kV as acceleration voltage. Fourier transform infrared spectra (FTIR) were derived from Perkin Elmer Fourier Transform Infrared Spectrometer GX. The XRD patterns of all samples were collected on XRD-6000X-ray diffractometer (Cu K_α source) at a scan rate of 5˚ min^{-1}. UV–Vis diffuse reflectance spectra (DRS) were measured with Lambda 750 UV/Vis/NIR spectrophotometer (Perkin-Elmer, USA) using $BaSO_4$ as reference. Photoluminescence (PL) spectra were accomplished in solid with Shimadzu RF5301 Spectrofuorophotometer. The specific surface area was calculated from N_2 adsorption–desorption isotherms measured through Surface Area and Porosity Analyzer (Micromeritics, ASAP 2020) by using the Brunauer–Emmett–Teller (BET) equation. The surface hydrophilicity was measured by contact-angle (CA) measurement (Data Physics, OCA 15 Pro), the samples were pressed to be tablets for measurement.

2.5. Photocatalytic CO_2 reduction in biphase:

For the photocatalytic measurement, 3.0 wt.% of Pt as cocatalyst was loaded through wetness impregnation process. Typically, the prepared sample (100 mg) was mixed with the H_2PtCl_6 (1.0 mg/mL) solution, followed by ultrasonic treatment for 5 min to form a slurry. After 2-hour impregnation under vigorous stirring, excess water was removed by drying at 70 ˚C in oven. Afterwards, the obtained solid samples were treated by $NaBH_4$ reduction. Final products were washed thoroughly with distilled water to completely remove ions, separated via centrifugation, and dried at 70 ˚C. In a quartz reactor, 10 mg of the catalyst was dispersed in a mixture of 1 ml aqueous solution of $NaHCO_3$ (3 M) and 9 ml cyclohexene (or 9 ml toluene containing 2 mmol of 2-methyl-2-butene) After sonication the mixture became a milky suspension, sealed with rubber and purge with N_2 for 30 min to drive away the inner air. Afterwards, the reactor was placed under illumination of Xeon lamp (300 W, MAX-302, Asahi Spectra, USA). Reaction kinetics were monitored via analyses of the withdrawn gaseous samples at a given period by GC (Shimadzu 2010) equipped with FID and TCD detectors. Liquid product was determined and analyzed at the end of reaction by GC-MS (Agilent 5977B GC/MSD).

3. Results and discussion

3.1 Preparation and characterization of Py-PCN

The synthetic procedures of Py-PCN is illustrated in Scheme 1. The raw PCN (denoted as CN0) microspheres were synthesized through a solvothermal process at 200 oC by using cyanuric chloride (CC) and cyanamide (CA) as precursors. The surfaces of these microsphere are enriched with 1,3,5-triazine based oligomers that are not fully condensed,[19] which allows PyCC to be grafted onto the microsphere surface through further polymerization and condensation together with CC and CA in the secondary solvothermal process. As such, the final pyrene-moiety is expected to covalently link with the tri-s-triazine structure on the PCN surface, given the product as Py-PCN.

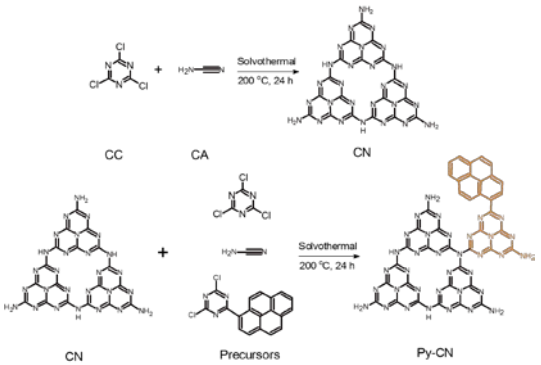

Scheme 1. Illustration of carbon nitride synthesis via solvothermal and further functionalization.

SEM images (Fig. 1a) indicate that the PCN products from the first solvothermal process are irregular sphere with diameters of 0.5~2.5 µm. After pyrene-functionalization, the morphology did not show obvious change, as shown in Fig. 1b. The XRD patterns (Fig. 2) of the obtained samples shows a clear peak at 27.3◦ (d ≈ 0.323 nm) corresponding to the (002) interlayer of graphitic carbon nitride. It indicates that the PCN product has well stacking of conjugated hexatomic heterocyclic system.[21] The FT-IR spectra (Fig. S1) also show the characteristic peaks of aromatic C-N heterocycles and s-triazine ring.

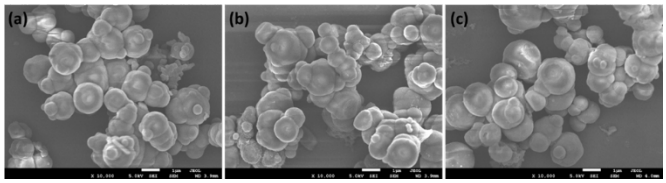

Fig. 1. SEM images of (a) CN0, (b) 0-PCN and (c) Py-PCN. The scale bar is 1 um.

While the microspheres do not show the characteristic peak of inplanar repeat packing at ≈ 13◦, suggesting the imperfect and disordered crystal structure of the PCN microspheres.[19] Functionalization of pyrene on the PCN surface by secondary solvothermal process did not clearly change the XRD pattern.

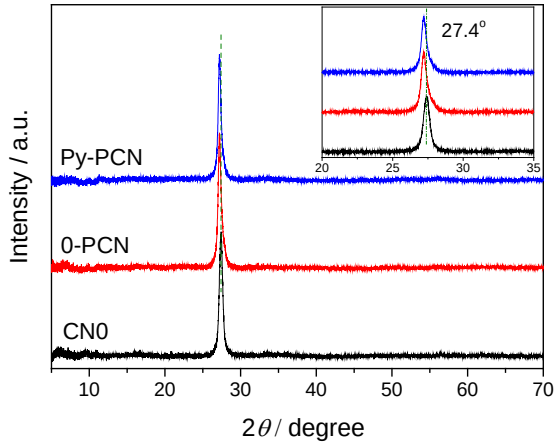

Fig. 2. XRD patterns of CN0, 0-PCN and Py-PCN.

The solid-state ^{13}C NMR spectra (Fig. 3) of Py-PCN show the two peaks at 154.0 and 162.3 ppm corresponding to the sp^2-hybridized carbon atoms of $-CN_2(NH_x)$ and $-CN_3$ in the CN network, respectively, which indicates the existence of characteristic tri-s-triazine structure.[22] Besides, the weak shoulder at ~157.6 ppm may be attribute to the junctional carbon atoms bridging the pyrene-moiety and two nitrogen atoms.[22] The signal at 123.1 ppm can be assigned to the aromatic carbon from pyrene moieties,[23] proving successful pyrene-functionalization. Elemental analysis results (Table S1) also indicate higher C/N ratio for Py-PCN as compared to 0-PCN.

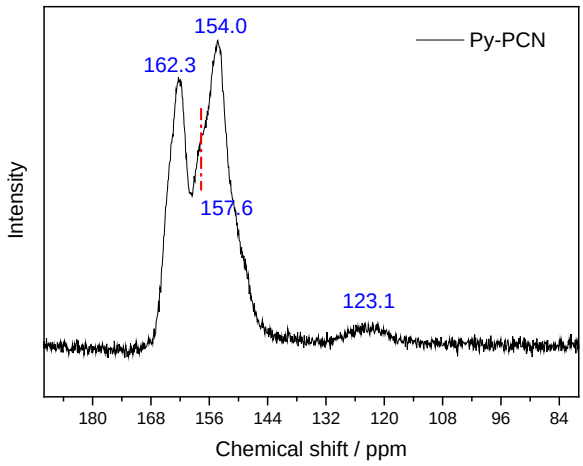

Fig. 3. Solid-state ^{13}C NMR spectra of Py-PCN.

3.2 Photocatalytic CO_2 reduction

The PCN based photocatalysts usually have sufficient conduction band level for CO_2 reduction into CO and various hydrocarbon products,[2] and have suitable valence band level, allowing the photogenerated holes to oxidize many different organic compounds in aqueous solution. However, their capability of initiating reaction with alkenes (C=C) is rarely investigated as most C=C enriched compounds are not soluble in water. In this study, the pyrene-functionalized carbon nitride allows affinity to both water and non-polar organic solvents. As such, we carry out photocatalytic tests in an aqueous-organic biphasic system by using bicarbonate in aqueous solution as the source for CO_2 reduction and alkene compounds in the organic phase for simultaneous reaction of C=C bond. The prepared PCN and Py-PCN samples were loaded with 3.0 wt.% Pt through wetness impregnation process, and suspended in the biphasic liquid for the photocatalytic reactions.[24]

3.2.1. Using cyclohexene

As a typical example, cyclohexene was used as both organic solvent and the reactant. In this case, CO was the predominant gaseous product. As shown in Fig. 4, comparing to the bare PCN sample (0-PCN), grafting with pyrene-moieties greatly enhanced the CO evolution rate up to 4 times (0.28 umol h^{-1} for 10% Py-PCN versus 0.07 umol h^{-1} for 0-PCN). The pyrene-

moieties afford hydrophobic characteristic and thus allow the Py-PCN surface to be more approachable by the cyclohexene molecules for reactions. The enhanced reaction process of cyclohexene promotes the reduction of bicarbonate by the photoelectrons in the aqueous phase. Nevertheless, the excessive pyrene-moieties would reduce the sample affinity to the aqueous phase. Thus we found that the 10% Py-PCN is the optimal sample (Fig. 4b).

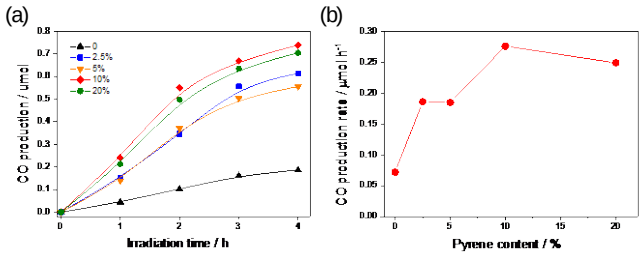

Fig. 4. (a) CO evolution time course over 0-PCN and Py-PCN with different content. Condition: [Cat.]=1.0 g/L; 9 ml cyclohexene as solvent and 1 ml of 3.0 M $NaHCO_3$ as CO_2 source. 300 W Xeon Lamp. (b) The relationship between CO generation rates versus pyrene content.

The control experiment (**#1**) showed no CO evolution over 4-hour irradiation when $NaHCO_3$ was absent in the aqueous phase. This indicates that the bicarbonate species serve as the source for CO production. We have also carried out an additional control experiment (**#2**) in aqueous solution only. As shown in Fig. 5, without cyclohexene, the CO evolution rate dropped more than 10 times, which proved that cyclohexene has significant contribution to the overall photocatalytic processes.

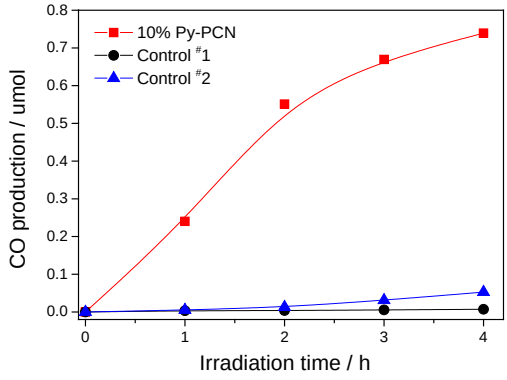

Fig. 5. Control experiments over 10% Py-PCN was carried out in the identical conditions except of free of $NaHCO_3$ and cyclohexene, respectively.

Further, we have examined the liquid products through GC-MS. Formic acid was the main product in the aqueous phase, and originates from HCO_3^- reduction by photoelectrons via multi-step electron transfer processes.[25, 26] Cyclohexanol was the main product in organic phase, and possibly produced through addition of water molecules. It is proposed that the C=C bond was firstly attacked by the •OH radical that was generated through oxidation of chemisorbed −OH by photogenerated holes on the PCN surface, followed by proton addition.[27] The reactivity of •OH radicals for addition of unsaturated C=C bonds has been extensively reported.[28,29] A possible reaction pathway for cyclohexene is elucidated in Fig. 6.

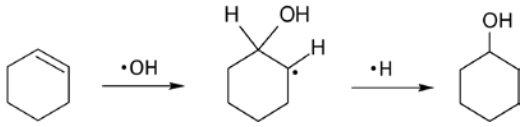

Fig. 6. Possible pathway of cyclohexene oxidation by hydroxyl radicals addition to C=C bond.

The quantification results after 4-hour irradiation are shown in Fig. 7. The 10% Py-PCN sample still exhibit much higher yield of formic acid (2.2 umol) and cyclohexanol (3 umol) than the bare PCN sample (0.37 umol formic acid and 1.1 umol cyclohexanol). Considering the CO evolution amount (0.76 umol for Py-PCN and 0.3 umol for the bare CN), the amount of photoelectrons that are consumed for reduction ($2n_{CO}$ + $2n_{HCOOH}$) is 5.92 umol over Py-PCN, which is close to the amount of photoholes for cyclohexene addition ($2n_{cyclohexanol}$) as 6.0 umol. This indicates that CO_2 reduction and cyclohexene addition are initiated and driven by photo-induced redox cycle. The small difference might be attributed to the trace amount of other liquid products, such as HCHO and CH_3CHO, which were hardly identified by our GC-MS.

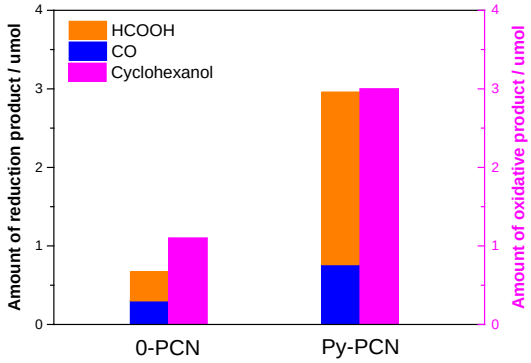

Fig. 7. Gaseous and liquid products comparison over 0-PCN and Py-PCN when using cyclohexene as substrate.

3.2.2. Using 2-methyl-2-butene

To further verify the hole oxidation capability of Py-PCN for C=C bond, we have carried out photoreduction of $NaHCO_3$ in aqueous solution with using 2-methyl-2-butene (2M2B) in toluene as organic phase. In this case, both CO and CH_4 were the main gaseous products, and no liquid reductive product was detected. Notably, the yield for CO and CH_4 over the 10% Py-PCN is about 4-fold and 7-fold higher of that over the bare PCN (Fig. 8). The main product in the liquid phase was identified as acetone, which is probably generated through oxidative addition of the C=C bond in 2M2B with water molecule by the •OH group created by the photogenerated holes on the PCN

surface.[30, 31] The process should have generated acetaldehyde simultaneously with the same molar amount of acetone, but acetaldehyde could not be accurately quantified in our GC-MS. In this reaction, the total amount of electrons for reduction ($2n_{CO} + 4n_{CH4}$) is almost equal to that of holes for addition ($2n_{Acetone}$) after 20 h irradiation (Fig. 9). Hence, it is reasonable to induce such a reaction pathway as shown in Fig. 10.

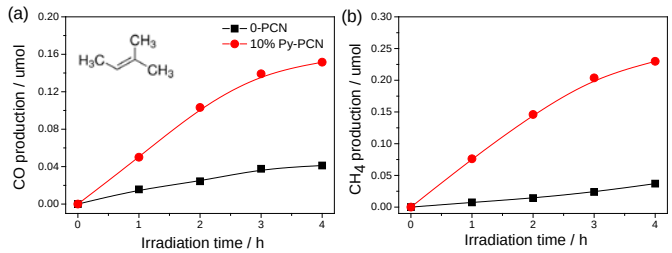

Fig. 8. CO (a) and CH_4 (b) evolution time course over 0-PCN and 10% Py-PCN, respectively. Condition: [Cat.]=1.0 g/L; 0.1 ml 2-methyl-2-butene in toluene and 1 ml of 3 M $NaHCO_3$ as CO_2 source. 300 W Xeon Lamp.

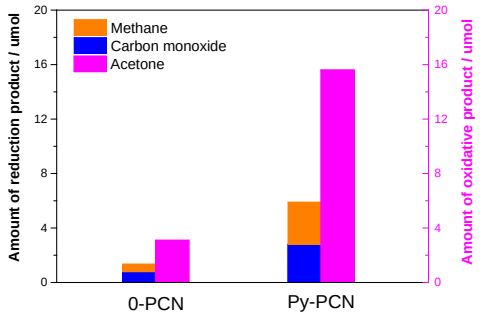

Fig. 9. Comparison of gaseous and liquid products between 0-PCN and Py-PCN using methyl-butene as substrate. The amount is accumulated after 20 h irradiation.

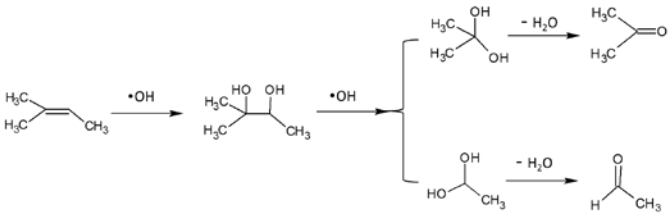

Fig. 10. The oxidation pathway of 2-methyl-2-butene by hydroxyl radicals.

The above photocatalytic experiments demonstrate that the C=C bond in organic alkenes can be indirectly reacted by the photogenerated holes of PCN when the photoelectrons are reducing HCO_3^-. Moreover, the pyrene-moiety grafted onto the PCN surface can promote adsorption of the hydrophobic organic alkenes as well as their addition with water, which enhances the overall photocatalytic activities.

Brunauer–Emmett–Teller (BET) surface area of 0-PCN and Py-PCN are measured by using liquid nitrogen adsorption–desorption isotherms (Fig. 11). The specific surface area of the Py-PCN was estimated as 2.11 $m^2\ g^{-1}$, which is lower than that of 0-PCN (5.49 $m^2\ g^{-1}$). The decrease of surface area after pyrene-moieties attachment can be attributed to the reduced surface roughness. The results further prove that the enhanced activity of Py-CN in the biphasic photocatalytic reaction is attributed to the surface pyrene-moieties, rather than effect of surface area.

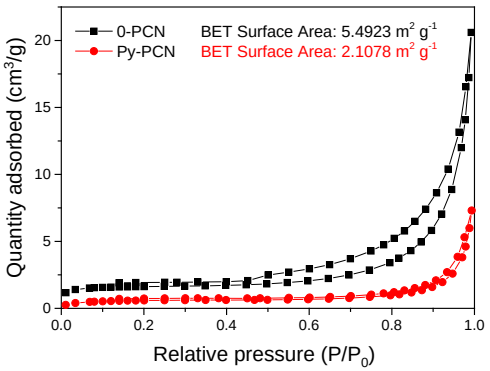

Fig. 11. The BET surface area calculated from nitrogen adsorption–desorption isotherms.

To clarify the effect of phase affinity on the photocatalytic activity, we have implemented a comparison experiment of photocatalytic H_2 generation in pure aqueous solution with 10% TEOA as hole scavenger, which is one of the most common reactions for identifying photocatalytic activity. Interestingly, the H_2 generation rate over the bare PCN was obviously higher than that over Py-PCN (Fig. 12), which is an opposite trend to the activities for bicarbonate reduction in the biphasic system. The lower photocatalytic activity of the Py-PCN in pure aqueous solution could be ascribed to the pyrene-moieties that restrict the free access of hydrophilic species, such as proton and TEOA, to the PCN surface, which reduces the rate of their redox reactions. The contact angle measurement confirmed that the Py-PCN is more resistant to water (Fig. S2). Therefore, we believe that the better performance of Py-PCN in the biphasic system would be more likely attributed to the increased hydrophobicity by the incorporated pyrene-moieties, rather than the improvement of electronic properties.

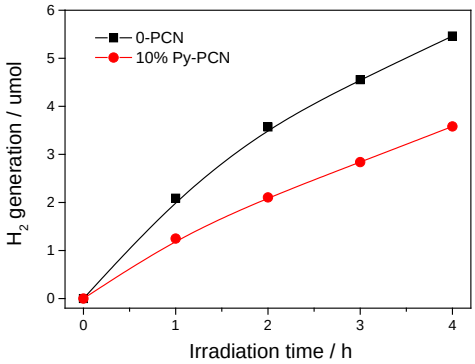

Fig. 12. Photocatalytic H_2 generation over 0-PCN and Py-PCN in aqueous solution. [Cat.] = 1.0 g/L with Pt 3.0 wt.% via impregnation; 10% TEOA as scavenger. Light source: Xe Lamp 300 W.

To verify this, we have identified the band energy levels for the Py-PCN and bare PCN (0-PCN). Fig. 13 shows the absorption spectra of 0-PCN and Py-PCN. According the K-M plot, the bandgap energies are estimated as 2.27 and 2.31 eV for the bare PCN and Py-PCN, respectively. The Mott-Schottky plot (Fig. S3)

was used to estimate the flatband potential of 0-PCN and Py-PCN as –0.85 V (vs. Ag/AgCl) and –0.94 V (vs. Ag/AgCl), respectively, which could be approximately regarded as the conduction band.[32] The detailed energy levels of conduction band and valance band (vs. NHE) were listed in Table S2. There is not much difference on the band structure between Py-PCN and bare PCN. And their conduction band potential is much more negative than the CO_2 reduction, thus it is thermodynamically favorable to produce different products. (Fig. S4)

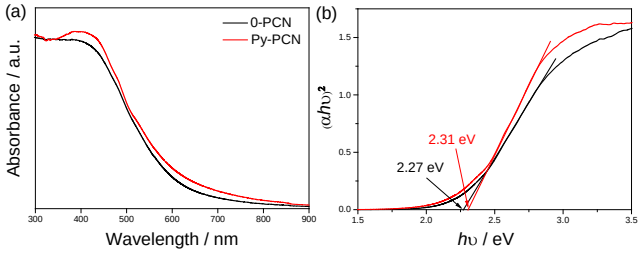

Fig. 13. (a) UV–Vis diffuse reflectance spectra of 0-PCN and Py-PCN. (b) Plot of transformed Kubelka–Munk function versus the energy of light.

The PL spectra (Fig. 14, excitation at 360 nm) reveal a slight blue shift for the emission peak of Py-PCN (479 nm) as compared to that of the bare PCN (485 nm), which is consistent with the slightly larger bandgap of Py-PCN.[33] Though the pyrene-CC precursor shows an intensive emission band at 488 nm, but it is quenched in the Py-PCN sample, suggesting strong π-π stacking existed between the pyrene and PCN. The results indicate that the pyrene-functionalization on PCN surface showed little change to the PCN band structure, had almost no effect on the charge separation and recombination on PCN.

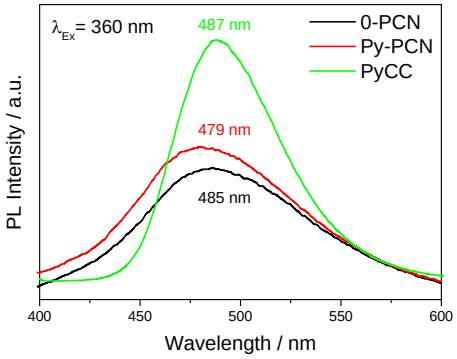

Fig. 14. PL spectra of 0-PCN, Py-PCN and PyCC with excitation wavelength of 360 nm.

3.3 Proposed reaction mechanism

The above results demonstrate that in the aqueous-organic biphasic system, the pyrene-functionalization of PCN endows certain lipophilic capability that enables the C=C bond of alkene compounds in the organic phase to readily approach the carbon nitride surface. Subsequently, the alkene molecules can sacrifice •OH radicals which are formed from oxidation of surface adsorbed -OH by the photogenerated holes (Fig. S5). This process promotes hole consumption, and consequently the charge separation efficiency is greatly improved, which allows the photoelectrons to be more effectively accumulated on the attached Pt catalyst surface for reduction of HCO_3^-. As such, the Py-PCN showed much better activity in the photocatalytic reduction of HCO_3^- in the biphasic system. In comparison, the bare PCN naturally has more hydrophilic surface covering with a water layer, which inhibits adsorption of hydrophobic alkenes. (Fig. 15) While the capability of holes for water oxidation towards oxygen evolution is very limited, resulting in low overall photocatalytic activity. So the role of pyrene-moiety is to optimize the interface of photocatalyst-organic solvent to promote the oxidation reaction, resulting in high charge separation efficiency for bicarbonate reduction. In addition, the cycling test (Fig. S6) indicates very good stability of Py-PCN for bicarbonate reduction.

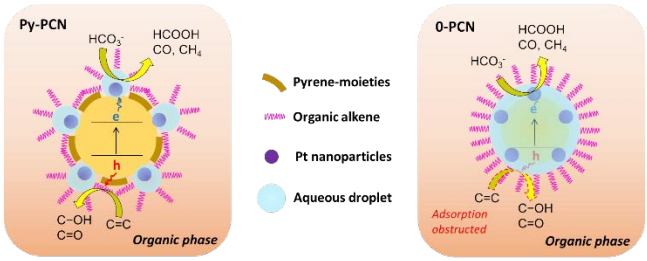

Fig. 15. Illustration of photocatalytic simultaneous CO_2 reduction and organic alkene (C=C) oxidation.

Conclusions

We have successfully grafted pyrene-functional groups on the PCN surface through a post co-polymerization strategy. Comparing the original bare PCN, the product, Py-PCN, exhibits greatly enhanced photocatalytic activities in an aqueous-organic biphasic environment, which enables efficient photoreduction of bicarbonate in the aqueous phase and simultaneous oxidation alkenes in the organic phase. The enhancement is attributed to the increased lipophilicity from the surface pyrene-functional groups that allows the hydrophobic organic molecules to readily approach the PCN surface and be reacted and converted to other molecules. This work is significant because of the unique promising advantages of biphasic photocatalytic reactions. Out studies demonstrate a new strategy for solar fuels production with effective utilization of the oxidization power of photo-holes for organic synthesis with convenient separation of the product in organic phase and economic solvent recovering.

Conflicts of interest

There are no conflicts to declare.

Acknowledgements

The authors acknowledge the financial support from NTU seed funding for Solar Fuels Laboratory, Singapore MOE AcRF-Tier1 (2016-T1-002-087, RG 120/16) and MOE AcRF-Tier2 (MOE2016-T2-2-056). M. Guan acknowledges the financial support from the National Natural Science Foundation of China (No. 21701057), Jiangsu Postdoctoral Research Funding Program (No. 1701109B), and China Postdoctoral Science Foundation (No. 2017M611708).

Notes and references

1 W. H. Wang, Y. Himeda, J. T. Muckerman, G. F. Manbeck and E. Fujita, *Chem. Rev*., 2015, **115**, 12936-12973.
2 M. G. Kibria and Z. Mi, *J. Mater. Chem. A*, 2016, **4**, 2801-2820.
3 Y. F. Guo, J. Li, Y. P. Yuan, L. Li, M. Y. Zhang, C. Y. Zhou, and Z. Q. Lin, *Angew. Chem. Int. Ed*., 2016, **55**, 14693-14697.
4 Q. Gu, H. Sun, Z. Xie, Z. W. Gao, and C. Xue, *Appl. Surf. Sci.*, 2017, **396**, 1808-1815.
5 H. Cheng, J. Hou, O. Takeda, X. M. Guo and H. Zhu, *J. Mater. Chem. A,* 2015, **3**, 11006-11013.
6 Y. He, L. Zhang, B. Teng and M. Fan, *Environ. Sci. Technol*., 2015, **49**, 649-656.
7 L. K. Putri, B.J. Ng, W.J. Ong, H. W. Lee, W. S. Chang and S. P. Chai, *J. Mater. Chem. A,* 2018, **6**, 3181-3194
8 J. Xu and M. Antonietti, *J. Am. Chem. Soc*., 2017,**139**, 6026-6029.
9 P. Xia, B. Zhu, J. Yu, S. Cao and M. Jaroniec, *J. Mater. Chem. A,* 2017, **5**, 3230-3238.
10 X. Liu, S. Inagaki and J. Gong, *Angew. Chem. Int. Ed*., 2016, **55**, 2-29.
11 Y. Pellegrin and F. Odobel, *Comptes Rendus Chimie*, 2017, **20**, 283-295.
12 Y. D. Li, Y. Q. Jiang, Z. H. Ruan, K. F. Lin, Z. B. Yu, Z. F. Zheng, X. Z. Xu, Y. Yuan, *J. Mater. Chem. A*, 2017, **5**, 21300-21312.
13 C. Chang, Y. Fu, M. Hu, C. Wang, G. Shan and L. Zhu, *Appl. Catal. B: Enviorn.*, 2013, **142-143**,553-560.
14 L. Lyu, L. Zhang, G. He, H. He and C. Hu, *J. Mater. Chem. A,* 2017, **5**, 7153-7164.
15 J. Low, J. Yu and W. Ho, *J. Phys. Chem. Lett*., 2015, **6**, 4244-4251.
16 J. Zhang, G. Zhang, X. Chen, S. Lin, L. Möhlmann, G. Dołęga, G. Lipner, M. Antonietti, S. Blechert and X. Wang, *Angew. Chem. Int. Ed.*, 2012, **51**, 3183-3187.
17 Y. Chen, J. Zhang, M. Zhang and X. Wang, *Chem. Sci*., 2013, **4**, 3244-3248.
18 Z. Chen, P. Sun, B. Fan, Q. Liu, Z. Zhang and X. Fang, *Appl. Catal. B: Environ.*, 2015, **170–171**, 10−16.
19 Q. Gu, Z. Gao and C. Xue, *Small* 2016, **12**, 3543-3549.
20 Q. Gu, X. Gong, Q. Jia, J. Liu, Z. Gao, X. Wang, J. Long, C. Xue *J. Mater. Chem. A* 2017, **5**, 19062-19071.
21 W. Ruland and B. Smarsly, *J. Appl. Crystallogr*., 2002, **35**, 624-633.
22 J. R. Holst and Edward. G. Gillan, *J. Am. Chem. Soc.,* 2008, **130**, 7373-7379.
23 K. C. Park, J. Cho and C. Y. Lee, *RSC Adv*., 2016, **6**, 75478-75481.
24 Q. Gu, Y. Liao, L. Yin, J. Long, X. Wang, C. Xue, *Appl. Catal. B: Environ.*, 2015, **165**, 503-510.
25 S. N. Habisreutinger, L. Schmidt-Mende and J. K. Stolarczyk, *Angew. Chem. Int. Ed*., 2013, **52**, 7372-7408.
26 N. Sreekanth and K. L. Phani, *Chem. Commun*., 2014, **50**, 11143-11146.
27 T. Berndt, S. Richters, T. Jokinen, N. Hyttinen, T. Kurtén, R. V. Otkjær, H. G. Kjaergaard, F. Stratmann, H. Herrmann, M. Sipilä, M. Kulmala and M. Ehn, *Nature Commun*., 2016, **7**, 13677.
28 J. H. Seinfeld and S. N. Pandis, Atmospheric Chemistry and Physics: from Air Pollution to Climate Change, third ed., Wiley/Interscience, New York, 1997.
29 H. Einaga, S. Futamura, T. Ibusuki, *Appl. Catal. B: Environ.,* 2002, **38**, 215-225.
30 D. J. M. Ray, R. R. Diaz and D. J. Waddington, Symposium (International) on Combustion 1973, **14**, 259-266.
31 D. J. M. Ray and D. J. Waddington, *Combustion and Flame*, 1973, **20**, 327-334.
32 Q. Li, Y. Xia, C. Yang, K. Lv, M. Lei and M. Li, *Chem. Eng. J*., 2018 **349**, 287-296.
33 Z. Song, Z. Li, L. Lin, Y. Zhang, T. Lin, L. Chen, Z. Cai, S. Lin, L. Guo, F. Fu and X. Wang, *Nanoscale*, 2017, **9**, 17737-17742.